Structural transition in the magnetoelectric $ZnCr_2Se_4$ spinel under pressure

I. Efthimiopoulos[1], Z. T. Y. Liu[2], S. V. Khare[2], P. Sarin[3], V. Tsurkan[4,5], A. Loidl[4], D. Popov[6], and Y. Wang[1]

[1]*Department of Physics, Oakland University, Rochester, Michigan 48309, USA*

[2]*Department of Physics, University of Toledo, Toledo, Ohio 43606, USA*

[3]*School of Materials Science and Engineering, Oklahoma State University, Tulsa, Oklahoma 74106, USA*

[4]*Institute of Applied Physics, Academy of Sciences of Moldova, MD-2028 Chisinau, Republic of Moldova*

[5]*Experimental Physics 5, Center for Electronic Correlations and Magnetism, Institute of Physics, University of Augsburg, D-86159 Augsburg, Germany*

[6]*High Pressure Collaborative Access Team, Geophysical Laboratory, Carnegie Institution of Washington, Argonne, Illinois 60439, USA*

SUPPLEMENTARY INFORMATION

Table S1: Assignments[1,2], frequencies, pressure coefficients, and the mode Gruneisen parameters γ of the Raman modes for the $Fd3\square m$ phase of $ZnCr_2Se_4$. The pressure depencence of the Raman-active modes is given by: $\omega(P)=\omega_0+\alpha P$, where frequency ω_0 is in cm^{-1} and pressure P in GPa. The Gruneisen parameters γ are determined from the relation: $\gamma=(B_0/\omega_0)x(\partial\omega/\partial P)$, where B_0=74.2 GPa (**Table I**).

Mode	ω_0 **(cm^{-1})**	$\partial\omega/\partial P$ **(cm^{-1}/GPa)**	**γ**
$F_{2g}(3)$	108.2	1	0.69
E_g	153.5	1.7	0.82
$F_{2g}(2)$	177	1.9	0.8
A_{1g}	232.9	3.7	1.18

Table S2: Experimentally determined structural data for the $Fd\bar{3}m$ (Z = 8) and the high-pressure monoclinic phases of $ZnCr_2Se_4$.

***Fd$\bar{3}$m*[a]**	***P*** **(GPa)**	***a*** **(Å)**	***V*** **(Å^3)**	**Se-u**	**Zn-Se (Å)**	**Cr-Se (Å)**	**Cr-Se-Cr (degrees)**
	10^{-4}	10.5005(1)	1157.79(3)	0.2598(4)	2.45(1)	2.53(1)	94.6(1)
	1.3	10.4420(1)	1138.56(3)	0.2604(4)	2.45(1)	2.51(1)	94.8(1)
	2.3	10.3983(1)	1124.31(3)	0.2606(4)	2.44(1)	2.49(1)	94.9(1)
	3.1	10.3685(1)	1114.67(3)	0.2602(4)	2.43(1)	2.49(1)	94.7(1)
	4.2	10.3284(1)	1101.79(3)	0.2602(4)	2.42(1)	2.48(1)	94.7(1)
	5.4	10.2872(1)	1088.67(3)	0.2599(4)	2.40(1)	2.47(1)	94.6(1)
	6.7	10.2419(1)	1074.35(3)	0.2599(4)	2.39(1)	2.46(1)	94.6(1)
	8.3	10.1957(1)	1059.87(3)	0.2596(4)	2.38(1)	2.45(1)	94.5(1)
	9.4	10.1605(1)	1048.92(3)	0.2595(4)	2.37(1)	2.45(1)	94.4(1)
	10.6	10.1262(1)	1038.34(3)	0.2591(4)	2.35(1)	2.44(1)	94.3(1)
	11.6	10.1018(1)	1030.85(3)	0.2595(4)	2.35(1)	2.43(1)	94.4(1)
	12.4	10.0794(1)	1024.02(3)	0.2595(4)	2.35(1)	2.43(1)	94.4(1)
	13.3	10.0594(1)	1017.93(3)	0.2595(4)	2.34(1)	2.42(1)	94.4(1)
	14.2	10.0349(1)	1010.53(3)	0.259(1)	2.34(1)	2.42(1)	94.3(2)
	15.1	10.012(1)	1003.6(3)	0.259(5)	2.33(1)	2.42(1)	94.2(2)
	16.7	9.96(1)	988(2)				
Monoclinic	***P*** **(GPa)**	***a*** **(Å)**	***b*** **(Å)**	***c*** **(Å)**	***β*** **(degrees)**	***V*** **(Å^3)**	
	18.3	11.1438(1)	6.8341(1)	13.197(1)	112.45(1)	929.24(8)	
	19.8	11.1216(1)	6.8098(1)	13.141(1)	112.78(1)	918.01(8)	
	21.4	11.0520(1)	6.7769(1)	13.093(1)	112.85(1)	904.07(8)	
	22.9	11.0119(1)	6.7297(1)	13.075(1)	113.03(1)	892.11(8)	
	24.7	10.9300(1)	6.6978(1)	12.990(1)	112.86(1)	876.59(8)	
	26.2	10.8979(1)	6.6902(1)	12.902(1)	112.94(1)	866.59(8)	
	28.2	10.8302(1)	6.6531(1)	12.828(1)	113.01(1)	851.14(8)	
	30	10.7731(1)	6.6373(1)	12.787(1)	112.66(1)	844.09(8)	

[a]**Wyckoff positions:** Zn (**8a**: 0.125, 0.125, 0.125), Cr (**16d**: 0.5, 0.5, 0.5), Se (**32e**: u, u, u)

Construction of the cubic and monoclinic paramagnetic structures of $ZnCr_2Se_4$

The paramagnetic cubic and monoclinic structures were obtained using the special quasi-random structure (SQS) generation algorithm[3,4] with a total of 56 atoms. A randomly distributed binary spin-up and spin-down Ising model was set up for Cr^{3+} to maintain a total of zero magnetic moments. The configuration space search tried to match pair clusters with a diameter of 7 Å and triplets with a diameter of 4 Å, and we collected one of the structures from four parallel copies of the stochastic search that ended up with the same lowest value of the objective function that showed no change after sufficient time. The detailed configurations are provided in **Tables S4 & S5**. The Γ-centered k-point mesh was selected so that the number of k-points per reciprocal atom (KPPRA) reached 1000 for both structures.

Table S3: Calculated structural parameters for the paramagnetic cubic and monoclinic phases of $ZnCr_2Se_4$ at various pressures. We note that the calculated structural parameters for the paramagnetic cubic phase are very close to the experimentally determined values; on the other hand, the respective values for the paramagnetic monoclinic phase exhibit deviations of ~3-4% compared to their experimental counterparts. Such differences are well-known effects within DFT calculations with GGA-PBE functionals. The employment of a hybrid functional study of magnetically randomized supercell structure would be computationally more demanding, therefore out of the scope of this work.

Paramagnetic cubic	***P* (GPa)**	***a* (Å)**				***V* (Å^3)**	***E* (eV)**
	-2.9	10.729				1235	-305.05
	1.4	10.516				1163	-305.38
	6.8	10.298				1092	-303.67
	13.6	10.069				1021	-299.16
	22.2	9.831				950	-291.31
Paramagnetic monoclinic	***P* (GPa)**	***a* (Å)**	***b* (Å)**	***c* (Å)**	***β* (degrees)**	***V* (Å^3)**	***E* (eV)**
	-4.7	13.309	7.517	14.179	115.54	1280	-297.29
	-2	12.759	7.511	13.732	115.79	1185	-299.80
	2	12.529	7.311	13.405	117.41	1090	-299.99
	7.9	11.937	7.014	13.165	115.49	995	-295.85
	16.8	11.566	6.721	12.785	115.11	900	-289.92
	23.3	11.389	6.556	12.559	115.13	849	-283.66
	30.3	11.239	6.408	12.365	115.31	805	-275.67

Table S4: Construction parameters for the special quasi-random structure (SQS) paramagnetic cubic $ZnCr_2Se_4$ supercell. The first half of the Cr cations are set to spin-up, and the second half spin-down. The cell parameters are unrelaxed as the starting point of the calculations.

Lattice vectors (Å)	x	y	z
a	-8.490	-8.490	0.000
b	-8.490	0.000	-8.490
c	0.000	-4.245	-4.245

Atom	Relative Coordinates			Atom	Relative Coordinates		
	u_1	u_2	u_3		u_1	u_2	u_3
Zn	0.438	0.438	0.875	Se	0.131	0.358	0.261
Zn	0.938	0.438	0.875	Se	0.631	0.358	0.261
Zn	0.438	0.938	0.875	Se	0.131	0.858	0.261
Zn	0.938	0.938	0.875	Se	0.631	0.858	0.261
Zn	0.063	0.063	0.125	Se	0.142	0.369	0.739
Zn	0.563	0.063	0.125	Se	0.642	0.369	0.739
Zn	0.063	0.563	0.125	Se	0.142	0.869	0.739
Zn	0.563	0.563	0.125	Se	0.642	0.869	0.739
Cr	0.500	0.250	0.500	Se	0.369	0.369	0.284
Cr	0.500	0.750	0.500	Se	0.869	0.369	0.284
Cr	0.250	0.250	0.500	Se	0.369	0.869	0.284
Cr	0.250	0.750	0.500	Se	0.869	0.869	0.284
Cr	0.250	0.250	1.000	Se	0.369	0.369	0.739
Cr	0.750	0.750	1.000	Se	0.869	0.369	0.739
Cr	0.250	0.500	0.500	Se	0.369	0.869	0.739
Cr	0.750	1.000	0.500	Se	0.869	0.869	0.739
Cr	1.000	0.250	0.500	Se	0.131	0.131	0.716
Cr	1.000	0.750	0.500	Se	0.631	0.131	0.716
Cr	0.750	0.250	0.500	Se	0.131	0.631	0.716
Cr	0.750	0.750	0.500	Se	0.631	0.631	0.716
Cr	0.750	0.250	1.000	Se	0.131	0.131	0.261
Cr	0.250	0.750	1.000	Se	0.631	0.131	0.261
Cr	0.750	0.500	0.500	Se	0.131	0.631	0.261
Cr	0.250	1.000	0.500	Se	0.631	0.631	0.261
				Se	0.369	0.142	0.739
				Se	0.869	0.142	0.739
				Se	0.369	0.642	0.739
				Se	0.869	0.642	0.739
				Se	0.358	0.131	0.261
				Se	0.858	0.131	0.261
				Se	0.358	0.631	0.261
				Se	0.858	0.631	0.261

Table S5: Construction parameters for the special quasi-random structure (SQS) paramagnetic monoclinic $ZnCr_2Se_4$ supercell. The first half of the Cr cations are set to spin-up, and the second half spin-down. The cell parameters are unrelaxed as the starting point of the calculations.

Lattice vectors (Å)	x	y	z
a	3.210	12.396	0.000
b	3.210	-12.396	0.000
c	0.000	-5.011	-10.780

Atom	Relative Coordinates			Atom	Relative Coordinates		
	u_1	u_2	u_3		u_1	u_2	u_3
Zn	0.250	0.250	1.000	Se	0.201	0.299	0.286
Zn	0.750	0.250	1.000	Se	0.701	0.299	0.286
Zn	0.250	0.750	1.000	Se	0.201	0.799	0.286
Zn	0.750	0.750	1.000	Se	0.701	0.799	0.286
Zn	0.250	0.250	0.500	Se	0.201	0.299	0.786
Zn	0.750	0.250	0.500	Se	0.701	0.299	0.786
Zn	0.250	0.750	0.500	Se	0.201	0.799	0.786
Zn	0.750	0.750	0.500	Se	0.701	0.799	0.786
Cr	0.620	0.380	0.342	Se	0.299	0.201	0.214
Cr	0.620	0.880	0.342	Se	0.799	0.201	0.214
Cr	0.120	0.380	0.842	Se	0.299	0.701	0.214
Cr	0.120	0.880	0.842	Se	0.799	0.701	0.214
Cr	0.880	0.120	0.158	Se	0.299	0.201	0.714
Cr	0.380	0.620	0.158	Se	0.799	0.201	0.714
Cr	0.880	0.120	0.658	Se	0.299	0.701	0.714
Cr	0.380	0.620	0.658	Se	0.799	0.701	0.714
Cr	0.120	0.380	0.342	Se	0.066	0.434	0.488
Cr	0.120	0.880	0.342	Se	0.566	0.434	0.488
Cr	0.620	0.380	0.842	Se	0.066	0.934	0.488
Cr	0.620	0.880	0.842	Se	0.566	0.934	0.488
Cr	0.380	0.120	0.158	Se	0.066	0.434	0.988
Cr	0.880	0.620	0.158	Se	0.566	0.434	0.988
Cr	0.380	0.120	0.658	Se	0.066	0.934	0.988
Cr	0.880	0.620	0.658	Se	0.566	0.934	0.988
				Se	0.434	0.066	0.012
				Se	0.934	0.066	0.012
				Se	0.434	0.566	0.012
				Se	0.934	0.566	0.012
				Se	0.434	0.066	0.512
				Se	0.934	0.066	0.512
				Se	0.434	0.566	0.512
				Se	0.934	0.566	0.512

Bonding and charge transfer in the cubic and monoclinic paramagnetic phases of $ZnCr_2Se_4$

To characterize the bonds between atoms, the projected Crystal Orbital Hamiltonian Populations (pCOHP)[5] were calculated using the program Local-Orbital Basis Suite Towards Electronic-Structure Reconstruction (LOBSTER)[6,7], carefully following its instructions on switching off symmetry, extra empty bands, and choice of basis functions[8]. For the ionic part of the analysis, Bader charge transfer analysis[9–11] was done with the implementation following theoretical guidelines[12–14], as described elsewhere[8,15–17]. The fast Fourier transform grid for charges was set at 500 × 500 × 300 for the cubic SQS supercell, and 500 × 500 × 500 for the monoclinic SQS supercell, proportional to the respective supercell geometry.

In the main text we discussed the pressure-dependent evolution of the bulk band gap E_g and the average magnetic moment μ of Cr^{3+} of the cubic and monoclinic phases. Here we examine the pressure-induced response of the Bader charge transfer q_{trans} of Cr^{3+} and the average integrated COHP (ICOHP) of the Cr-Se bond (**Fig. S1**) for both phases at various pressure values. Granted, the cubic phase beyond the transition point and the monoclinic phase below it correspond to 'unstable' states when compared to each other. Nevertheless, the study of these states in their full pressure range offers valuable insight on the evolution of their properties. We should mention that the absolute values of q_{trans} under the Bader charge division scheme are usually smaller than the chemical notations would imply, but the trend that relies on relative values is still meaningful[8,15]. We note also that the ICOHP is a quantity proportional to the bond strength, i.e. the more negative it becomes, the stronger (more covalent) the bond gets.

As we can observe, compression of the cubic spinel phase leads to the gradual decrease of all the above quantities. The same rule applies to the monoclinic phase. A notable exception is the slightly increasing ICOHP of the Cr-Se bond in the cubic phase [**Fig. S1(e), black line**]. Since the value of ICOHP reflects the bonding and anti-bonding contributions, we can interpret this behavior as follows: when pressure increases, the two contributions cancel each other out (with slightly dominating anti-bonding contributions), leading to this ICOHP value increase. On the other hand, the decreasing trend of Cr^{3+} μ closely correlates with the behavior of the Cr^{3+} charge transfer q_{trans} [**Figs. S1(c, d)**]. In particular, the reduction of q_{trans} under pressure suggests that less and less electrons are transferred away from the Cr^{3+} cations, i.e. more and more electrons fill in the Cr-*d* states upon pressure increase. Since the 3*d* spin electrons of Cr^{3+} reside in the t_{2g} orbitals, some of the additional electrons that fill in the Cr-*d* states under pressure will pair up and reduce the net magnetic moment. This effect is not seen in the case of $CoCr_2O_4$, where both the average charge transfer and magnetic moment of Cr^{3+} undergo minimal changes under pressure[18]. We believe that this is due to the stronger hybridization of the more extended Se-*p* orbitals with the Cr-*d* states in $ZnCr_2Se_4$, compared to the O-*p* orbitals in $CoCr_2O_4$.

Upon passing into the structural stability regime of the monoclinic phase, i.e. beyond 13 GPa, we can observe significant changes in each of the calculated physical quantities [**Fig. S1, from black to red line at transition point**]. Besides the bulk band gap reduction (**Fig. 6**), the magnetic moment μ of Cr^{3+} becomes alost halved, whereas the ICOHP of the Cr-Se bond drops also upon the cubic-monoclinic transition. The latter suggests a more covalent character for the Cr-Se interatomic bond in the high-pressure monoclinic phase.

As for the substantial μ drop at the transition point (~13 GPa), it cannot be accounted for solely by the reduction of q_{trans}. Hence, we look into the pressure evolution of the monoclinic phase, even before the transition point. We speculate that the Cr-Se bond strengthening (ICOHP decrease) should also contribute to the significant decrease of μ. The effect of ICOHP on the magnetic moment μ can be easily understood, since the enhancement of the Cr-Se bond covalency leads to the draining of the Cr^{3+} 3*d* spin electrons and, therefore, to the subsequent drop of μ. This mechanism is additive to that of q_{trans}, whose reduction under pressure requires more electrons filling in the Cr-*d* states. In order to get a qualitative validation of our assumption, we have averaged over the two competing effects on μ [**Fig. S1(f)**]. Despite the crude and naive approximation of linear summation involved in plotting, it manages to reproduce satisfactorily the trend of μ under pressure for both phases. Hence, we can state that both charge transfer and covalency effects should be taken into account for determining the magnitude of μ in this system.

We mention in passing that the monoclinic phase exhibits an abrupt drop in each of the calculated quantities between 3-8 GPa, outside its experimental stability regime. Careful inspection of the monoclinic EOS curve reveals a sample point sitting slightly above the curve near 3-8 GPa [**Fig. S1(a)**]; a similar break is also detected in the monoclinic lattice parameters (**Fig. S2**). This “anomaly” leads to a volume compressibility change, hinting a second-order transition of the monoclinic phase.

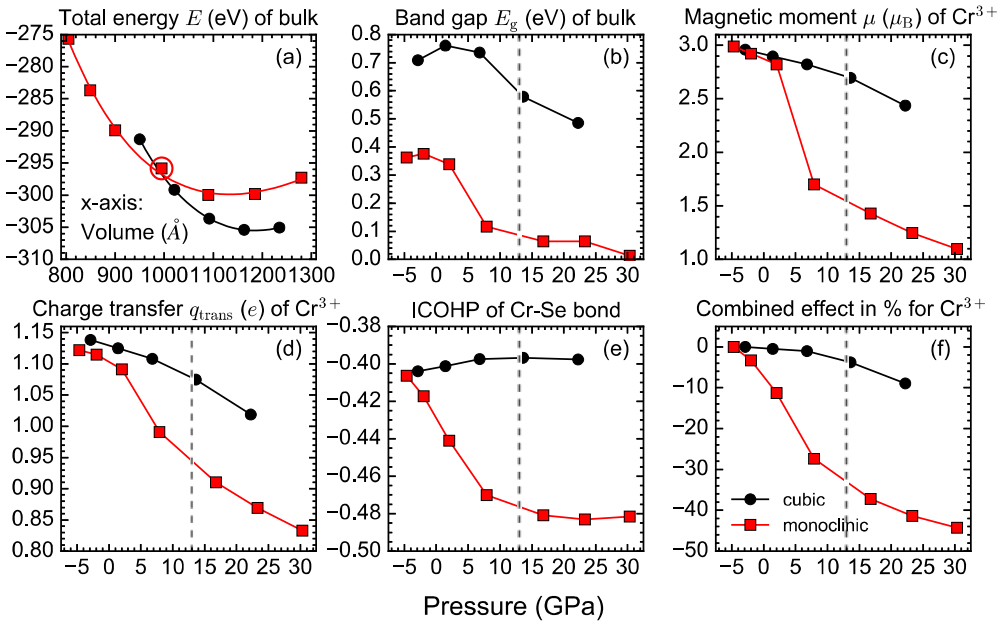

FIG. S1: (a), (b) Bulk and (c), (d), (e), (f) microscopic quantities related to Cr^{3+} in the paramagnetic cubic and monoclinic phases of $ZnCr_2Se_4$ as a function of pressure [except in (a) where the x-axis is volume]. (a) A sample point of the monoclinic phase at ~1000 Å (in red circle) sits slightly above the EOS fitting curve, suggesting a possible transition within the monoclinic phase. (b), (c), (d), (e), (f) The band gap E_g of bulk, the average magnetic moment μ of Cr^{3+}, the Bader charge transfer of Cr^{3+}, the ICOHP of the Cr-Se bond of the monoclinic phase experience a sharp drop between 3-8 GPa, and the combined effect in (d) and (e).

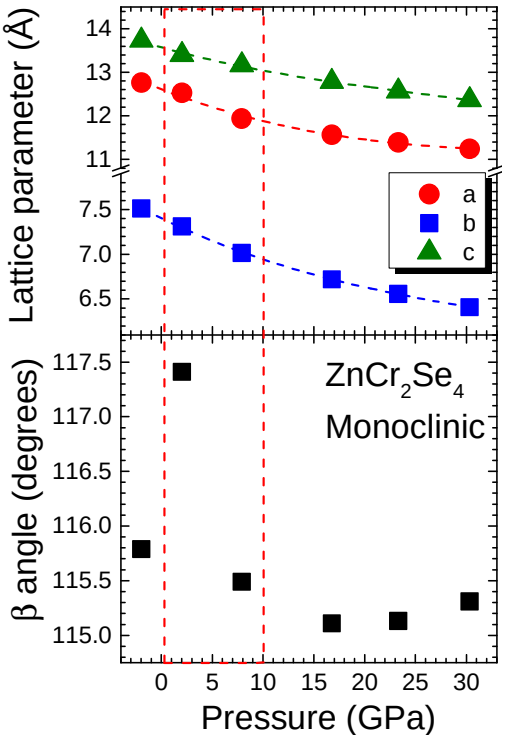

FIG S2: Evolution of the DFT calculated lattice parameters for the monoclinic phase of $ZnCr_2Se_4$ under pressure. The section in the red rectangular frame indicates the possible *isostructural* transition.

REFERENCES

[1] A.K. Kushwaha, Commun. Theor. Phys. **50**, 1422 (2008).

[2] J. Zwinscher and H.D. Lutz, J. All. Comp. **219**, 103 (1995).

[3] A. Zunger, S.H. Wei, L.G. Ferreira, and J.E. Bernard, Phys. Rev. Lett. **65**, 353 (1990).

[4] A. van de Walle, P. Tiwary, M. de Jong, D.L. Olmsted, M. Asta, A. Dick, D. Shin, Y. Wang, L.-Q. Chen, and Z.-K. Liu, Calphad-Computer Coupling Phase Diagrams Thermochem. **42**, 13 (2013).

[5] R. Dronskowski and P.E. Blochl, J Phys Chem **97**, 8617 (1993).

[6] V.L. Deringer, A.L. Tchougreeff, and R. Dronskowski, J Phys. Chem. A **115**, 5461 (2011).

[7] S. Maintz, V.L. Deringer, A.L. Tchougreeff, and R. Dronskowski, J. Comput. Chem. **34**, 2557 (2013).

[8] Z.T.Y. Liu, D. Gall, and S. V Khare, Phys. Rev. B **90**, 134102 (2014).

[9] R.F.W. Bader, *Atoms in Molecules: A Quantum Theory* (Oxford University Press,

New York, 1990).

[10] F.W. Bieglerkonig, R.F.W. Bader, and T.-H. Tang, J. Comput. Chem. **3**, 317 (1982).

[11] F.W. Bieglerkonig, T.T. Nguyendang, Y. Tal, R.F.W. Bader, and A.J. Duke, J. Phys. B-At. Mol. Opt. Phys. **14**, 2739 (1981).

[12] G. Henkelman, A. Arnaldsson, and H. Jonsson, Comput. Mater. Sci. **36**, 354 (2006).

[13] E. Sanville, S.D. Kenny, R. Smith, and G. Henkelman, J. Comput. Chem. **28**, 899 (2007).

[14] W. Tang, E. Sanville, and G. Henkelman, J Phys. Cond. Matt. **21**, 84204 (2009).

[15] Z.T.Y. Liu, X. Zhou, D. Gall, and S. V Khare, Comput. Mater. Sci. **84**, 365 (2014).

[16] Z.T.Y. Liu, X. Zhou, S. V Khare, and D. Gall, J. Phys. Cond. Mat. **26**, 25404 (2014).

[17] J.L. Roehl, Z.T.Y. Liu, and S. V Khare, Mater. Res. Express **1**, 25904 (2014).

[18] I. Efthimiopoulos, Z.T.Y. Liu, S. V Khare, P. Sarin, T. Lochbiler, V. Tsurkan, A. Loidl, D. Popov, and Y. Wang, Phys. Rev. B **92**, 064108 (2015).